On Condensation and Evaporation in Turbulence Cloud Parameterizations

SHOUPING WANG

Universities Space Research Association, Huntsville, Alabama

QING WANG

Naval Postgraduate School, Monterey, California

16 October 1998 and 5 April 1999

ABSTRACT

An analysis of the condensation and evaporation processes involved in the classic Sommeria–Deardoff–Mellor turbulence cloud models is presented. A liquid water budget is derived from the diagnostic Gaussian cloud relations. It is found that the adiabatic condensation generated by turbulent eddies at the cloud base and the mean radiative cooling at the cloud top are the two major processes responsible for the condensation in the parameterizations for stratocumulus-topped boundary layers. The evaporation is directly related to the stratification of the boundary layers and the turbulence variability (variance and covariance) of the conserved thermodynamic variables. The evaporation caused by the turbulence variability plays a dominant role at the cloud top. The analysis also shows that the profile of the parameterized liquid water flux is primarily determined by the turbulence-generated condensation and evaporation in the cloud model. This model is also compared with other prognostic cloud schemes.

1. Introduction

The turbulence cloud parameterizations developed by Sommeria and Deardorff (1977) and Mellor (1977) have been widely used in various turbulence closure models of cloud-topped boundary layers. This type of parameterization describes clouds by specifying the distribution of fluctuating moisture departure from saturation. In essence, the method defines the condensation–evaporation (CE) rate produced by the mean as well as turbulence fields, which is at the heart of any cloud parameterization. However, the CE rate does not explicitly appear in the parameterizations because they are usually used in a diagnostic form. Some studies (e.g., Smith 1990; Sommeria and Deardorff 1977) used similar cloud parameterizations in a prognostic form to calculate the net CE rate, which, however, cannot identify each physical component that contributes to the CE.

In recent years, many prognostic approaches have been proposed to define clouds in large-scale or turbulence closure models. These methods include highly complicated explicit bin microphysical models, like that of Bott et al. (1996), as well as relatively simple ones like that of Tiedtke (1993). Despite the different complexity in the model cloud processes, an essential question in all the prognostic methods is how one should relate the CE processes to the mean and turbulence fields.

In this note, we do not intend to investigate the CE processes in real clouds. Rather, we will provide new insight into the CE processes in the turbulence cloud parameterization by Sommeria and Deardorff (1977) and Mellor (1977). Particularly, we will focus on how the CE is parameterized in terms of the mean and turbulence fields. We will first derive an analytical expression for the CE rate from the diagnostic cloud relations and then discuss individual components in the CE parameterization based on a numerical simulation. Finally, we will make further comments on liquid water flux and comparisons with other prognostic cloud schemes.

2. Derivation

To derive the CE rate, one may use a one-dimensional budget of liquid water content (LWC) in a generic form,

$$\frac{\partial \overline{q_l}}{\partial t} = -\overline{w}\frac{\partial \overline{q_l}}{\partial z} - \frac{\partial \overline{w' q_l'}}{\partial z} + \mathrm{CE}, \tag{1}$$

where q_l is LWC, w vertical velocity, and an overbar denotes an ensemble average. Before introducing the cloud parameterization, we define following variables. Saturation water vapor mixing ratio at mean liquid water

Corresponding author address: Shouping Wang, Universities Space Research Association, Global Hydrology and Climate Center, 977 Explorer Blvd., Huntsville, AL 35806.
E-mail: wangsx@vmcs.msfc.nasa.gov

temperature is $\overline{q_{sl}} = q_s(\overline{T_l}, \overline{p})$, where $T_l = T - q_l L c_p^{-1}$. The normalized mean moisture departure from the saturation is defined as

$$Q_1 = \frac{\overline{q_t} - \overline{q_{sl}}}{\sigma_s}, \tag{2}$$

where

$$\sigma_s^2 = \overline{q_t'^2} - 2\frac{c_p\gamma}{L}\frac{\overline{T}}{\overline{\theta}}\overline{q_t'\theta_l'} + \left(\frac{c_p\gamma}{L}\frac{\overline{T}}{\overline{\theta}}\right)^2\overline{\theta_l'^2} \quad \text{with}$$

$$\gamma = \frac{L}{c_p}\frac{\partial\overline{q_{sl}}}{\partial T_l}. \tag{3}$$

With above definitions, Bougeault (1982) gave the following diagnostic relations for the turbulence cloud parameterization:

$$C = \int_{-Q_1}^{\infty} G(u)\, du; \tag{4}$$

$$\overline{q_l} = \frac{\sigma_s}{(1+\gamma)}\int_{-Q_1}^{\infty}(Q_1 + u)G(u)\, du; \tag{5}$$

and the liquid water flux,

$$\overline{w'q_l'} = \frac{C}{1+\gamma}\left(\overline{w'q_t'} - \frac{c_p\gamma}{L}\frac{\overline{T}}{\overline{\theta}}\overline{w'\theta_l'}\right), \tag{6}$$

where C is cloud fraction, and G a probability density function (PDF) of the random variable u essentially representing normalized fluctuating LWC and available vapor. It is important to notice that $\overline{q_l}$ and C may be defined with any specified PDF for G in (4) and (5), while the turbulent flux by (6) is only strictly derived for a Gaussian PDF (Mellor 1977). Therefore, the derivation of the CE rate presented below is correct only for a Gaussian PDF. Although some studies have provided empirical and more generalized turbulence cloud models (e.g., Bougeault 1982; Bechtold and Siebesma 1998), no attempt is made in this note to include those parameterizations.

The approach here is to derive a prognostic equation for $\overline{q_l}$ from (5) and then compare its individual terms with those in (1) to obtain the CE term. Note that in (4) and (5), u is an independent variable and $G(u)$ is independent of t and z. In addition, $Q_1(t, z)$ defined by (2) is independent of u. We thus differentiate (5) with respect to time by applying the generalized Leibniz rule (see appendix A) and obtain

$$\frac{\partial\overline{q_l}}{\partial t} = \frac{1}{1+\gamma}\left\{\frac{\partial\sigma_s}{\partial t}\int_{-Q_1}^{\infty}(Q_1+u)G(u)\, du + \sigma_s\left[\int_{-Q_1}^{\infty}\frac{\partial Q_1}{\partial t}G(u)\, du + \frac{\partial Q_1}{\partial t}(Q_1 - Q_1)G(-Q_1)\right]\right\}, \tag{7}$$

where γ is considered to be constant with time and the last term is, of course, zero. We use (2)–(3) to derive a $\partial Q_1/\partial t$ and rewrite (7) as

$$\frac{\partial\overline{q_l}}{\partial t} = \left(\overline{q_l} - \frac{\Delta qC}{1+\gamma}\right)\frac{1}{2\sigma_s^2}\frac{\partial\sigma_s^2}{\partial t} + \frac{C}{1+\gamma}\left[\frac{\partial\overline{q_t}}{\partial t} - \frac{c_p\gamma}{L}\frac{\overline{T}}{\overline{\theta}}\frac{\partial\overline{\theta_l}}{\partial t} - \left(\frac{\gamma R\overline{T_l}}{L} - \overline{q_{sl}}\right)\frac{1}{\overline{p}}\frac{\partial\overline{p}}{\partial t}\right], \tag{8}$$

where $\Delta q = \overline{q_t} - \overline{q_{sl}}$. One can easily show that the pressure tendency term is negligibly small compared with other terms due to the hydrostatic approximation for the mean pressure. The tendencies of $\overline{q_t}$ and $\overline{\theta_l}$ in (8) should be replaced by their prognostic equations. [See, e.g., Wang and Wang (1994). In this note, precipitation process is not considered.] We then differentiate (5) with respect to z and obtain the large-scale advection term:

$$-\overline{w}\frac{\partial\overline{q_l}}{\partial z} = -\overline{w}\left(\overline{q_l} - \frac{\Delta qC}{1+\gamma}\right)\frac{1}{2\sigma_s^2}\frac{\partial\sigma_s^2}{\partial z} - \overline{w}\frac{C}{1+\gamma}\left[\frac{\partial\overline{q_t}}{\partial z} - \frac{c_p\gamma}{L}\left(\frac{\overline{T}}{\overline{\theta}}\frac{\partial\overline{\theta_l}}{\partial z} - \frac{\overline{T_l}}{\overline{T}}\frac{g}{c_p}\right) - \frac{\overline{q_{sl}}g}{R\overline{T_l}}\right]. \tag{9}$$

In the above equation and following derivations, $\overline{T_l}/\overline{T} \cong 1$ is used.

We rearrange and regroup the terms on the rhs of (8) to give the advection term defined by (9) and the liquid water flux divergence defined by the vertical gradient of (6)[1] to obtain

[1] The factor $c_p\gamma\overline{T}(\overline{\theta}\ L)^{-1}$ in (6) is a weak function of height and considered independent of height in the derivation.

$$\frac{\partial\overline{q_l}}{\partial t} = -\overline{w}\frac{\partial\overline{q_l}}{\partial z} - \frac{\partial\overline{w'q_l'}}{\partial z} + \left\{\frac{C}{(1+\gamma)}\frac{c_p\gamma}{L}\frac{\partial F_R}{\partial z} + \frac{\overline{w}Cg}{(1+\gamma)}\left(\frac{\gamma}{L} - \frac{\overline{q_{sl}}}{R\overline{T_l}}\right) + \frac{1}{1+\gamma}\left(\overline{w'q_t'} - \frac{c_p\gamma}{L}\frac{\overline{T}}{\overline{\theta}}\overline{w'\theta_l'}\right)\frac{\partial C}{\partial z} + \left(\overline{q_l} - \frac{\Delta qC}{1+\gamma}\right)\frac{1}{2\sigma_s^2}\left(\frac{\partial\sigma_s^2}{\partial t} + \overline{w}\frac{\partial\sigma_s^2}{\partial z}\right)\right\}, \tag{10}$$

where the F_R is the radiative flux. Comparing the terms on the rhs of (10) with those of (1), one clearly sees that the {•} term in (10) represents the CE rate. We further derive the gradient of C using (4), substitute it into (10), and finally obtain the CE rate in the following form:

$$\mathrm{CE} = \mathrm{CE1} + \mathrm{CE2} + \mathrm{CE3}, \tag{11}$$

where

$$\mathrm{CE1} = \frac{\overline{w}C}{(1+\gamma)}\left(\frac{\gamma}{L} - \frac{\overline{q_{sl}}}{R\overline{T_l}}\right)g + \frac{C}{(1+\gamma)}\frac{c_p\gamma}{L}\frac{\partial F_R}{\partial z} \tag{12}$$

$$\mathrm{CE2} = \frac{1}{1+\gamma}\left(\overline{w'q_t'} - \frac{c_p\gamma}{L}\frac{\overline{T}}{\overline{\theta}}\overline{w'\theta_l'}\right)\frac{G(-Q_1)}{\sigma_s} \times \left[\underbrace{\left(\frac{\gamma}{L} - \frac{\overline{q_{sl}}}{R\overline{T_l}}\right)g}_{1} + \underbrace{\left(\frac{\partial\overline{q_t}}{\partial z} - \frac{c_p\gamma}{L}\frac{\overline{T}}{\overline{\theta}}\frac{\partial\overline{\theta_l}}{\partial z}\right)}_{2} + \underbrace{\left(-\frac{\Delta q}{2\sigma_s}\frac{\partial\sigma_s^2}{\partial z}\right)}_{3}\right] \tag{13}$$

and

$$\mathrm{CE3} = \left(\overline{q_l} - \frac{\Delta qC}{1+\gamma}\right)\frac{1}{2\sigma_s^2}\frac{d\sigma_s^2}{dt}, \tag{14}$$

where $d/dt \equiv \partial/\partial t + \overline{w}\partial/\partial z$. The term CE1 is related to the large-scale vertical motion and radiation and does not directly involve turbulence variables; CE2 is derived from the gradient of cloud fraction and is directly related to turbulence CE; CE3 represents the effects of the variance (σ_s^2) generation on the CE rate. CE2 can be further decomposed into three terms (as indicated by the three numbers below the equation) that will be discussed in detail in the next section.

3. Cloud processes

In this section, we present an example of the LWC budget defined by (10) and discuss how individual terms in (12)–(14) contribute to the net CE rate based on a simulation of stratocumulus-topped boundary layer. For this purpose, we include the cloud parameterization with a Gaussian PDF [i.e., $G = (2\pi)^{-1}\exp(-u^2)$ in (4) and (5)] in the third-order turbulence closure model used by Wang and Wang (1994). This model is coupled with the four-stream radiation parameterization developed by Fu et al. (1995). We choose the case of the stratocumulus-topped boundary layer used in the first Global Energy and Water Experiment Cloud System Study workshop. The complete model setup, large-scale fields, initial conditions, and discussion of results can be found in Moeng et al. (1996) and Bechtold et al. (1996). The only difference between our model setup and theirs is that we use 20 m for the grid spacing while they used 25 m. The model was run for 5 h and all the analyses were conducted over the last hour with the data sampled at each time step.

There are two ways to calculate the net CE rate. One is to use (11)–(14) without using the budget (1), a diagnostic approach; the other is to include the budget (1) and use the LWC definition (5) to calculate the CE rate, a prognostic approach. These two approaches should give the same results for the CE rate and for all the cloud variables. Both approaches are used in our calculations. For the prognostic approach, all the dynamic processes (turbulence, radiation, and large-scale advection except the cloud parameterization) in all of the equations are performed first at each time step to give an intermediate value of LWC $q_l^*(t)$, and then (5) is used to calculate $\overline{q_l}(t)$ based on the updated mean and turbulence structure. Clearly, the difference between $\overline{q_l}(t)$ and $q_l^*(t)$ is solely due to CE processes, and then the CE rate can be calculated as

$$[\mathrm{CE}] = \frac{\overline{q_l}(t) - q_l^*(t)}{\Delta t}, \tag{15}$$

where Δt is the time step (5 s).

a. The LWC budget

As shown in Fig. 1a, the three cloud variables ($\overline{q_l}$, C, and $\overline{w'q_l'}$) derived from the cloud scheme have profiles typical of stratocumulus-topped boundary layers and are similar to those shown in Moeng et al. (1996) and Bechtold et al. (1996). Figure 1b shows the $\overline{q_l}$ budget. The net CE rates derived from (15) and from (11)–(14) closely match each other, giving confidence in the derivation. Clearly, the flux divergence and the CE term are in reasonable balance. The subsidence advection term is important only at the cloud top where $\overline{q_l}$ rapidly decreases to zero from its maximum. The net CE rate is positive above the cloud base and reaches its maximum just 70 m higher, indicating that significant condensation occurs at that level. In the middle of the cloud layer where $C \cong 1$, the CE rate is small since it is related to the gradient of cloud fraction. Near the top of the cloud, CE becomes large and negative, reaching the minimum value of -40 g kg^{-1} day^{-1} at 750 m, indicating very strong evaporation there. In the meantime, the flux divergence term is negative below 720 m, implying that the liquid water produced by the CE term below is trans-

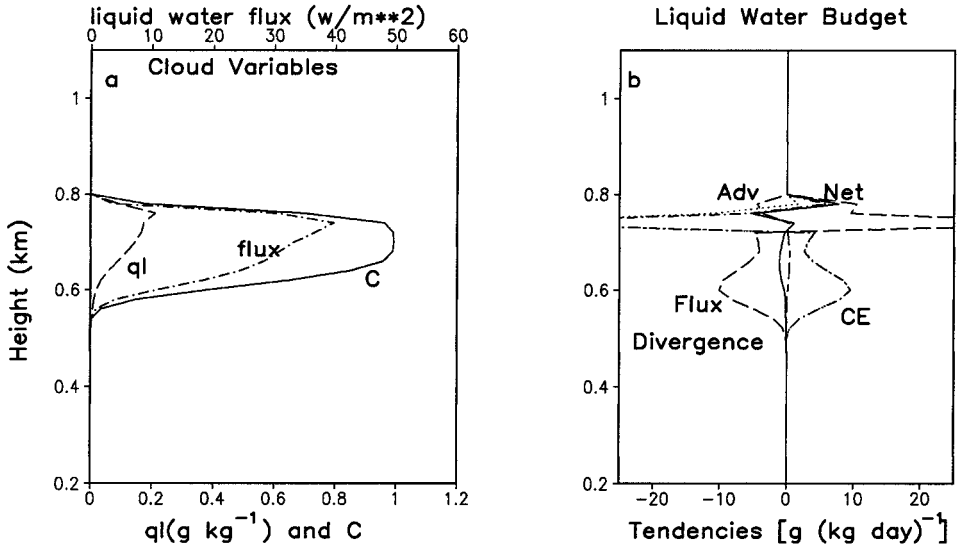

FIG. 1. Cloud variables and LWC budget. (a) $\overline{q_l}$ (g kg^{-1}), $L\rho\overline{w'q_l'}$ (W m^{-2}), and C; (b) dash–dotted line represents the net CE rate calculated from (11)–(14), dotted the CE from (15), long dashed the flux divergence, long–short dashed vertical advection, and solid the net tendencies derived from the budget (11). Note that the net CE rates computed using the two methods are very similar.

ported upward. At the cloud top, the convergence of the flux balances the evaporation. This picture of the LWC budget is basically consistent with our general understanding of the cloud generation and dissipation processes. Since the CE term represents only the net rate, we need to look into the individual terms in (12)–(14) to understand how it is related to the various mean and turbulence fields.

b. The condensation and evaporation processes

We further decompose CE1, CE2, and CE3 into the individual terms, which are shown in Figs. 2a,b. Appendix B shows that $g[\gamma/L - \overline{q_{sl}}/(R\overline{T_l})](1 + \gamma)^{-1}$ is approximately equal to the gradient of saturation water vapor mixing ratio following a mean moist adiabat. Thus, the first term in CE1 defined by (12) describes

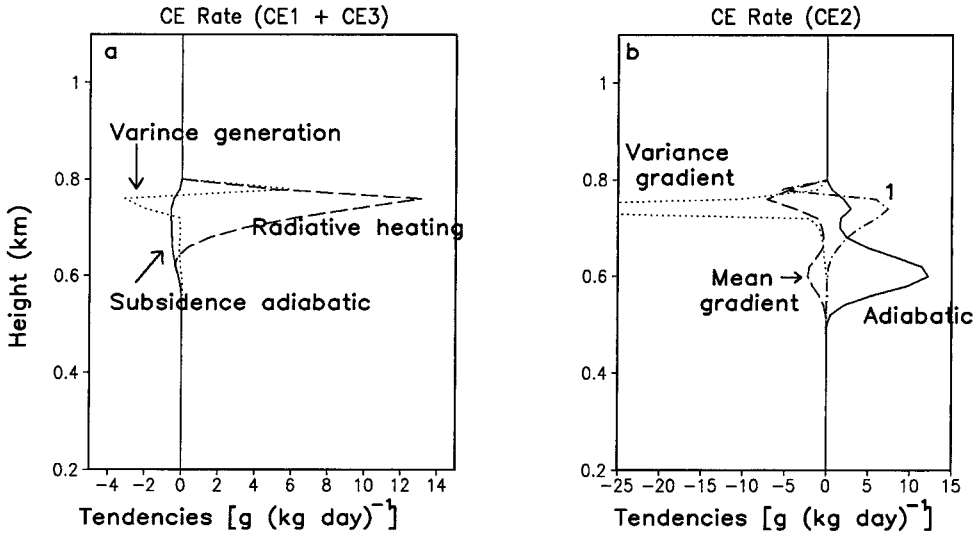

FIG. 2. Condensation and evaporation components. (a) CE1 and CE3; solid line denotes the moist-adiabatic large-scale subsidence term (CE1), dashed the radiative heating (CE1), and dotted the variance generation (CE3) terms; (b) terms in CE2; solid line represents the turbulence adiabatic condensation rate, dashed the mean gradient term, and dotted the variance gradient term. The number ''1'' denotes the first term in (16).

condensation or evaporation by large-scale vertical motion following the mean moist adiabat. Clearly, this term is negative due to the subsidence in the simulation. The second term represents the effects of radiative process: the longwave cooling at the cloud top contributes significantly to condensation, while the effect of the cloud-base warming is limited. Thus, CE1 is the CE rate produced by the mean fields.

Both CE2 and CE3 are produced by turbulent processes, as they are directly associated to the turbulent fluxes and variances. As seen in (10), CE2 is related to vertical gradient of the cloud fraction. We have further expressed this gradient in terms of gradients of the mean and turbulence variables, which actually define an ensemble of turbulent eddies following different thermodynamic paths. Therefore, CE2 can be represented by the three terms inside the square bracket in (13), multiplied by the factor $[\overline{w'q_t'} - (c_p\gamma/L)(\overline{T}/\overline{\theta})\,\overline{w'\theta_l'}](1 + \gamma)^{-1}$, which is always positive for the marine boundary layer. The first term describes the moist-adiabatic motion and makes a major positive contribution at the cloud base, as shown in Fig. 2b. This term decreases upward and has a second maximum just below the cloud top. The second term and the third terms describe impacts of nonadiabatic paths of turbulent eddies. Obviously, the decrease of $\overline{q_t}$ or increase of $\overline{\theta_l}$ with height in the inversion causes negative contribution (or evaporation) to the CE rate. The variance gradient term gives most contribution to the evaporation near the cloud top where the mean condition is still saturated (by which we mean $\Delta q = \overline{q_t} - \overline{q_{sl}} \geq 0$). It is because the increase of the variability with height means that more turbulent eddies follow the paths that diverge from the mean saturation. It is important to notice that the turbulence condensation–evaporation by (13) is strongly regulated by $G(-Q_1)$, which has maxima at $\Delta q = 0$ for the Gaussian PDF. Thus, condensation starts where the mean condition is still below saturation (i.e., $\Delta q = \overline{q_t} - \overline{q_{sl}} < 0$) and the evaporation starts where the mean is still saturated; and both condensation and evaporation reach their own maxima where the mean condition is *just* saturated. The cloud-top entrainment strongly affect the gradients of the mean and the turbulence variables, and thus it also significantly affects these negative contributing terms. It is interesting to note that the adiabatic condensation term [i.e., term 1 in (13)] has a similar profile as those of positive supersaturation calculated in some coupled large eddy simulation (LES) and bin-microphysics models such as in Kogan et al. (1995).

The variance-generation term (*CE3*) defined by (14) is positive at the cloud top due to the production of σ_s there, because stronger turbulence under relatively dry mean conditions means that some extreme eddies may become moist and cool enough to get saturated. This condensation is important, since it represents the growth of the cloud top.

The above analysis clearly demonstrates that, at the cloud base, the adiabatic condensation by turbulent eddies offsets the negative contributions by the gradient terms to result in a net condensation there. Near the cloud top, the negative contributions by the gradients of the mean and the variance dominate among all the terms, leading to the net evaporation there. This analysis of the CE profile shown in Fig. 1b, is consistent with the classic condensation theory.

We can summarize the major cloud processes in the parameterization for this simulation as follows. At the cloud base, turbulent eddies following the mean moist adiabat initiate condensation to form the clouds; the turbulence transports liquid water upward to the cloud top where the mean radiative cooling significantly enhances the condensation. In the meantime, evaporation occurs as a result of the stratification of the cloud layer. In the middle of the cloud layer, both the condensation and evaporation rates reach a minimum because the air at the levels is almost everywhere saturated and no water vapor excess or deficit is present. At the cloud top, evaporation is significant due to the increase of the variance σ_s^2 and it balances the turbulent flux convergence at the cloud top.

4. Further comments

One of the important features of the liquid water flux profile is that it is positive in the entire cloud layer (Fig. 1a) for the marine boundary layers. Clearly, this positive liquid water flux cannot be explained by any diffusion type of parameterizations, as discussed by Stevens et al. (1998). We may gain more insight into the liquid water flux profile by differentiating (6) with respect to z to obtain

$$\frac{\partial \overline{w'q_l'}}{\partial z} \cong \frac{C}{1+\gamma}\frac{\partial}{\partial z}\left(\overline{w'q_t'} - \frac{c_p\gamma}{L}\frac{\overline{T}}{\overline{\theta}}\overline{w'\theta_l'}\right) + \frac{1}{1+\gamma}\left(\overline{w'q_t'} - \frac{c_p\gamma}{L}\frac{\overline{T}}{\overline{\theta}}\overline{w'\theta_l'}\right)\frac{\partial C}{\partial z}. \quad (16)$$

The first term, displayed in Fig. 2b., represents the turbulence dynamics as it is related to the gradients of the turbulent fluxes of the conserved variables; the second term clearly represents the turbulence-generated CE as it is the same as CE2, whose different components are also shown in Fig. 2b. We clearly see that the turbulence CE term (i.e., CE2) dominates due to the adiabatic condensation at the cloud base and the evaporation due to the variance gradient at the top, although in the middle of the cloud layer the two terms are approximately equal. In general, the gradients of $\overline{w'q_t'}$ can be positive, negative, or even zero depending on the turbulence dynamics, even though the liquid water flux is always positive in the marine boundary layers. Thus, the main process that defines the vertical profile of the liquid water flux is the turbulence CE in this cloud parameterization.

Furthermore, substituting (16) to (10) and cancelling the second term in (16) with the CE2 term, we have

$$\frac{\partial \overline{q_l}}{\partial t} = -\overline{w}\frac{\partial \overline{q_l}}{\partial z} - \frac{C}{1+\gamma}\frac{\partial}{\partial z}\left(\overline{w'q_t'} - \frac{c_p\gamma}{L}\frac{\overline{T}}{\overline{\theta}}\overline{w'\theta_l'}\right) + \text{CE1} + \text{CE3}. \quad (17)$$

Thus, CE2 drops out the budget and only the mean CE term (CE1) and the turbulence variance production term (CE3) contribute to the net CE rate. The cancellation between the major parts of the flux divergence and turbulence condensation comes as no surprise, because vertical motion and cloud microphysics are closely coupled. For a well-mixed stratocumulus case as presented here, there are no significant θ_l and q_t variances except near the cloud top. Therefore, the mean condensation term CE1 dominates in (17). This is why some one-dimensional models (e.g., Bott et al. 1996) that include only the mean condensation due to the radiation (not turbulence condensation processes) still produce reasonable $\overline{q_l}$ profiles in stratocumulus clouds. If the boundary layer becomes stratified as in the case of decoupled stratocumulus clouds, significant variances will develop particularly at the cloud base. In that scenario, the variance production term CE3 can no longer be neglected and may give important contribution to the net CE rate.

Of many cloud prognostic parameterizations, Tiedtke's (1993) scheme stands out as it explicitly parameterizes *each* individual process contributing to condensation and evaporation, and to the flux transport. Despite differences in the detailed formulation between the Tiedtke's scheme and the one discussed in this note, the cloud processes considered in both schemes are similar. For condensation, Tiedtke includes the processes of moist-adiabatic convective upward motion, defined by convective updraft mass flux, and radiative cooling, which are equivalent to the two individual terms in CE1 and CE2. For evaporation, Tiedtke's scheme includes moist-adiabatic subsidence warming and evaporation due to turbulence mixing in an unsaturated environment, which should correspond to the terms of (12) and (13). Tiedtke formulated the evaporation due to turbulence mixing in terms of the mean saturation deficit and an evaporation timescale, while the turbulence cloud scheme uses turbulent fluxes and the gradient of conserved variables and their variance and covariance. It suggests that the timescale in the Tiedtke's scheme is related to the environmental turbulence structure. The detrainment of liquid water from the updrafts in the Tiedtke's scheme should correspond to part of the liquid water flux divergence term in the budget (10).

One unique feature of the Tiedtke's scheme is the use of prognostic equations for both C and $\overline{q_l}$ with one-to-one correspondence between the terms in these two equations. One may also derive a prognostic relation for C from (4). We first differentiate (4) with respect to time, then compare the result with the prognostic equation for $\overline{q_l}$, and finally obtain the following:[2]

$$\frac{\partial C}{\partial t} = \frac{G(-Q_1)}{C}\frac{\partial}{\partial t}\left[\frac{(1+\gamma)\overline{q_l}}{\sigma_s}\right]. \quad (18)$$

In the above equation, function G can be any PDF, since only (4) and (5) are used in the derivation. Thus, in principle, (18) can be used for any type of clouds. This equation states that the tendency of C is proportional to that of the normalized liquid water $[\overline{q_l}(1+\gamma)\sigma_s^{-1}]$. Therefore, each of the cloud processes discussed for the $\overline{q_l}$ budget in the previous section directly contributes to the changes in C, which is consistent with Tiedtke's approach. In addition, C is a decreasing function of σ_s. It is because for same $\overline{q_l}$ [which is a function of both σ_s and $(\overline{q_t} - \overline{q_{sl}})$ for a given PDF], an increase in σ_s means that more liquid water needs to be condensed in fewer turbulent eddies. Thus, a smaller cloud fraction results. Furthermore, (18) suggests that the cloud fraction tendency is directly related to the liquid water flux divergence being distributed by σ_s, while Tiedtke's scheme only relates the tendency to the mass flux divergence. Although the derivation of (18) is specifically based on (4) and (5), it provides some useful ideas on how a prognostic equation for C should be formulated in general.

We also notice that $G(-Q_1) \to 0$ for either $Q_1 \to -\infty$ (i.e., $C = 0$) or $Q_1 \to +\infty$ (i.e., $C = 1$); and it reaches maximum when $Q_1 = 0$ (i.e., $C = 0.5$) for a symmetric PDF. Figure 3 demonstrates the similarity between the profiles of $C(1 - C)$ and the various functions of $G(-Q_1)$ for the simulated structure. Thus, it is reasonable to express $G(-Q_1)$ in terms of C, for example, $G(-Q_1) \cong kC(1 - C)$, where k is an adjustable parameter. Substituting it to (18) and performing the integration, one has the following diagnostic relation between C and $\overline{q_l}$:

$$C = 1 - \exp\left[-k\frac{(1+\gamma)\overline{q_l}}{\sigma_s}\right]. \quad (19)$$

One may use observations or LES data to evaluate (19) and determine the parameter k. This expression can be used with diagnostic or prognostic $\overline{q_l}$. For example, it is possible to use Tiedtke's scheme to predict $\overline{q_l}$ and then compute C using (19). One advantage of the diagnostic relationship is that C is directly linked to $\overline{q_l}$, a nice physical constraint. The disadvantages are that values of k are likely to be different for different types of clouds and σ_s is difficult to obtain in a large-scale meteorological model.

Finally, a comprehensive understanding of a cloud

[2] For the Gaussian PDF, $G(-Q_1)/C \to +\infty$ with $Q_1 \to -\infty$. However, the singularity disappears when the liquid water budget is substituted in (18). For either the exponential or the positively skewed PDFs, $G(-Q_1)/C$ approaches a fixed constant with $Q_1 \to -\infty$.

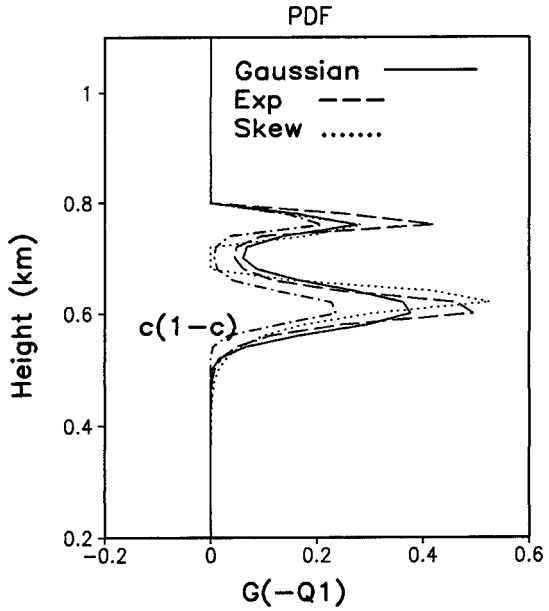

FIG. 3. Profiles of $G(-Q_1)$ and $C(1 - C)$. The exponential PDF is defined by $G = (1/\sqrt{2})e^{-\sqrt{2}|u|}$; the positively skewed PDF is $G = H(u + 1)e^{-(u+1)}$, where H is Heaviside function. The functions of $G(-Q_1)$ are calculated with the same Q_1 profile calculated by the model.

model is critical if it is to be used to study real physical processes in clouds. We believe that this study not only provides more understanding of the classic turbulence condensation theory, but also gives implications for future development of the new parameterizations.

Acknowledgments. We appreciate the comments of Charlie Cohen and Bob Haney on the original manuscript. Bjorn Stevens provided constructive suggestions on the discussion of the condensation and evaporation processes. Three anonymous reviewers are thanked for their thorough reviews. Shouping Wang was supported by NASA/FIRE III and EOS programs. Qing Wang was supported by NSF Grant ATM 9700845.

APPENDIX A

Leibniz's Rule

Following Kaplan (1973, 287–288, 447–448), one may express the generalized Leibniz rule as

$$\frac{d}{dt}\int_{g(t)}^{\infty} f(u, t)\, du = \int_{g(t)}^{\infty} \frac{\partial f(u, t)}{\partial t}\, du - f[g(t), t]\frac{dg(t)}{dt}. \tag{A1}$$

APPENDIX B

Approximated Moist-Adiabatic Water Vapor Mixing Ratio Gradient

In the cloud model, we need to compute $q_s(T, p)$ in terms of T_l. Thus, the saturated water vapor mixing ratio is approximated as

$$q_s(T, p) \cong q_s(T_l, p) + \frac{\partial q_s(T_l, p)}{\partial T_l}(T - T_l)$$
$$\cong q_{sl} + \gamma[q_t - q_s(T, p)]. \tag{B1}$$

We then can compute the gradient of the water vapor mixing ratio for moist-adiabatic process as follows:

$$\left.\frac{\partial q_s}{\partial z}\right|_{\text{adiabatic}} \cong \frac{1}{1 + \gamma}\left.\frac{\partial q_{sl}}{\partial z}\right|_{\text{adiabatic}}$$
$$\cong -\frac{g}{1 + \gamma}\left[\frac{\gamma}{L} - \frac{q_{sl}}{RT_l}\right]. \tag{B2}$$

REFERENCES

Bechtold, P., and P. Siebesma, 1998: Organization and representation of boundary layer clouds. *J. Atmos. Sci.,* **55,** 888–895.

——, S. K. Krueger, W. S. Lewellen, E. V. Meijaard, C.-H. Moeng, D. A. Randall, A. van Ulden, and S. Wang, 1996: Modeling a stratocumulus-topped PBL: Intercomparison among different 1D codes and with LES. *Bull. Amer. Meteor. Soc.,* **77,** 2033–2042.

Bott, A., T. Trautmann, and W. Zdunkowski, 1996: A numerical model of the cloud-topped planetary boundary layer. Radiation, turbulence and spectral microphysics in marine stratus. *Quart. J. Roy. Meteor. Soc.,* **122,** 635–667.

Bougeault, P. H., 1982: Cloud-ensemble relations based on the gamma probability distribution for the higher-order models of the planetary boundary layer. *J. Atmos. Sci.,* **39,** 2691–2700.

Fu, Q., S. K. Krueger, and K. N. Liou, 1995: Interactions of radiation and convection in simulated tropical cloud clusters. *J. Atmos. Sci.,* **52,** 1310–1328.

Kaplan, W., 1973: *Advanced Calculus.* 2d ed. Addison-Wesley, 709 pp.

Kogan, Y. L., M. P. Khairoutdinov, D. K. Lilly, Z. N. Kogan, and Q. Liu, 1995: Modeling of stratocumulus cloud layers in a large eddy simulation model with explicit microphysics. *J. Atmos. Sci.,* **52,** 2923–2940.

Mellor, G. L., 1977: The Gaussian cloud model relations. *J. Atmos. Sci.,* **34,** 356–358.

Moeng, C.-H., and Coauthors, 1996: Simulation of a stratocumulus-topped planetary boundary layer: Intercomparison among different numerical codes. *Bull. Amer. Meteor. Soc.,* **77,** 261–278.

Smith, R. N. B., 1990: A scheme for predicting layer clouds and their water content in a general circulation model. *Quart. J. Roy. Meteor. Soc.,* **116,** 435–460.

Sommeria, G., and J. W. Deardorff, 1977: Subgrid-scale condensation in models of nonprecipitating clouds. *J. Atmos. Sci.,* **34,** 344–355.

Stevens, B., W. R. Cotton, and G. Feingold, 1998: A critique of one and two-dimensional models of marine boundary layer clouds with detailed representations of droplet microphysics. *Atmos. Res.,* **47–48,** 529–553.

Tiedtke, M., 1993: Representation of clouds in large-scale models. *Mon. Wea. Rev.,* **121,** 3040–3061.

Wang, S., and Q. Wang, 1994: Roles of drizzle in a one-dimensional third-order turbulence closure model of the nocturnal stratus-topped marine boundary layer. *J. Atmos. Sci.,* **51,** 1559–1576.